Dispersion of Rayleigh, Scholte, Stoneley and Love waves in a model consisting of a liquid layer overlying a two-layer transversely isotropic solid medium

Amirhossein Bagheri,[1] Stewart Greenhalgh,[2] Ali Khojasteh[1] and Mohammad Rahimian[1]

[1]*Department of Civil Engineering, University of Tehran, Tehran, Iran. E-mail: rahimian@ut.ac.ir*

[2]*Institute of Geophysics, ETH Zurich, 8092 Zurich, Switzerland*

SUMMARY

The dispersion of interface waves is studied theoretically in a model consisting of a liquid layer of finite thickness overlying a transversely isotropic solid layer which is itself underlain by a transversely isotropic solid of dissimilar elastic properties. The method of potential functions and Hankel transformation was utilized to solve the equations of motion. Two frequency equations were developed: one for Love waves and the other for the remaining surface and interface waves. Numerical group and phase velocity dispersion curves were computed for four different classes of model, in which the substratum is stiffer or weaker than the overlying layer, and for various thickness combinations of the layers. Dispersion curves are presented for generalized Rayleigh, Scholte, Stoneley and Love waves, each of which are possible in all proposed models. They show the dependence of the velocity on layer thicknesses and material properties (elastic constants). Special cases involving zero thickness for the water layer or the solid layer, and/or isotropic material properties for the solid exhibit interesting features and agree favourably with previously published results for these simpler cases, thus validating the new formulation.

Key words: Surface waves and free oscillations; Interface waves; Seismic anisotropy; Theoretical seismology; Wave propagation; Acoustic properties.

1 INTRODUCTION

The study of propagation of dispersive surface and interface waves arises in numerous fields, including seismology, earthquake engineering, geophysics, materials testing and medical imaging. The problem has been tackled by many scientists from various points of view. Waves in layered media involving solid–solid interfaces, liquid–solid interfaces or those of both kinds are important due to their multiple applications. The layered solid half-space is often the background medium of interest in materials science, geophysical investigations, soil structure interactions, where one may encounter generalized Rayleigh waves at the free surface, and Love waves and—under rather stringent conditions—Stoneley waves at the interface of two solids. Stoneley (1924), Haskell (1953) and Ewing *et al.* (1957) were some of the first researchers who dealt with this kind of problem. In many situations, such as oceanic modelling for seabed characterization, fluid–soil–structure interactions, subsurface defect detection and elucidating the properties of a liquid layer one has to take account of solid and fluid media which are in contact. At the interface between a liquid layer and a solid half-space (e.g. the ocean floor), the interacting Rayleigh and Scholte (Stoneley) waves should be taken under consideration. Amongst the early researchers, Stoneley (1926), Biot (1952) and Tolstoy (1954) presented noteworthy works about the effect of the liquid layer on wave propagation in such media.

To date, more complicated cases and several methods for analysing such waves and their applications in the aforementioned fields of science and engineering have arisen. The subject has been investigated from an experimental, theoretical as well as numerical approach, and appropriate solutions devised (Ostoja-Starzewski 1987; Kerner *et al.* 1989; Favretto-anres & Rabau 1997; Padilla *et al.* 1999; Zhou & Greenhalgh, 2008; Zhou *et al.* 2009, 2012; Boxberger *et al.* 2011; Flores-Mendez *et al.* 2012; Nadri *et al.* 2012; Kiełczyński *et al.* 2014 and many others). The medium complexities introduced in the literature since the early pioneering work have included a number of interacting liquid and solid layers, material anisotropy, viscosity of the liquid, heterogeneity of the material and porosity of the solid. Transverse isotropy with a vertical axis of symmetry (VTI medium) is a common assumption made in many solid–solid and liquid–solid models involving

anisotropy, such as in a layered Earth and oceanic crustal models. There is ample field and laboratory evidence that certain minerals such as beryl have an intrinsic microcrystalline anisotropy of this form (Crampin, 1981) or that a sequence of alternating isotropic layers behave macroscopically as a pseudo-anisotropic unit which can be described as a VTI solid. This is sometimes referred to as structural anisotropy. Consequently, such materials have been the subject of a wide range of investigations.

The notable effect of transverse isotropy of materials on elastic wave propagation was first studied by Stoneley (1949), and Synge (1957); later Buchwald (1961) and Payton (1983) tackled the problem of elastodynamics of such a material. Rahimian *et al.* (2007) presented the analytic solution for the response of a three dimensional transversely isotropic half-space to a general, time-harmonic surface loading. Khojasteh *et al.* (2008a) extended the previous work to represent explicit expressions for the dynamic Green's functions in a transversely isotropic half-space and continued the work for full spaces comprised of two and three dissimilar materials, as well as two-layered and multilayered half-spaces (Khojasteh *et al.* 2008b,c, 2011, 2013). A transversely isotropic bed in contact with a liquid layer was first studied by Abubakar & Hudson (1961). Many years later, Sharma *et al.* (1990, 1991) deduced the frequency (dispersion) equation for Rayleigh type surface waves on a model consisting of a liquid layer lying over a solid layer which itself is underlain by a solid half-space. Sharma in a separate paper (1999) presented the wave dispersion characteristics in an ocean crust model incorporating the effect of cracks. Unlike this study, the propagation described in (Sharma *et al.* 1990, 1991; Sharma 1999) is two-dimensional and also required that one of the solid layers be isotropic. Numerical results were presented for just one specific model in each case, and Love waves were not considered.

In this contribution, we examine the phase and group velocity dispersion characteristics of surface waves for a half-space consisting of a liquid layer overlying a transversely isotropic solid layer which in turn overlies a transversely isotropic solid half-space of different material properties. Rayleigh and Scholte waves interacting at the liquid–solid interface and Stoneley waves at the solid–solid interface are studied where the latter, unlike a liquid–solid interface, arises only under rare conditions. Also, we investigate the Love wave dispersion associated with a solid layer above a half space. Due to the inviscid liquid assumption, no distortional interaction is possible between the middle layer and the liquid layer; and hence, the liquid layer has no effect on the Love wave.

Following the work of Rahimian *et al.* (2007) and Khojasteh *et al.* (2008a,b,c, 2011), the method of potential functions with an integral transformation of the Hankel type has been adopted to deal with the equations of motions and to derive the frequency equations. The arrival times of the waves depend on the elastic properties of the layers and so it is possible (although not specifically investigated here) to reverse the reasoning and tackle the inverse problem of deducing the structure of the medium from the dispersion characteristics; this is of major importance in marine seismology and geophysical investigations. The formulation can also be extended to derive Green's functions of the stress, displacement and fluid pressure fields for a source in the specified model. There is some inconsistency in the literature as to the terminology for interface waves, and so to avoid confusion hereafter we use the names 'Scholte waves', which is the term suggested by Cagniard (1962), and 'Stoneley waves' to denote the liquid–solid and solid–solid interface waves, respectively.

2 STATEMENT OF THE PROBLEM AND GOVERNING EQUATIONS

The model under consideration, shown in Fig. 1, comprises a compressible liquid layer overlying a homogeneous transversely isotropic solid layer of finite thickness, which sits above a uniform half space of dissimilar transversely isotropic properties. The fluid layer is of thickness h and that of the underlying solid layer is h'. In this section we give a brief analysis of the governing equations. The reader is referred to (Rahimian *et al.* 2007) for a more complete and detailed treatment.
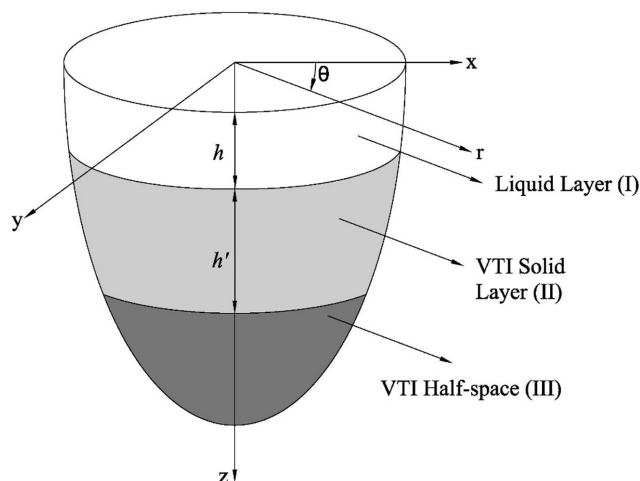

Figure 1. Model configuration.

For the homogeneous transversely isotropic solid layers, the time-harmonic equations of motion for the vector displacement **u** in cylindrical co-ordinates (r, θ, z) are:

$$c_{11}\left(\frac{\partial^2 u_r}{\partial r^2} + \frac{1}{r}\frac{\partial u_r}{\partial r} - \frac{u_r}{r^2}\right) + c_{66}\frac{1}{r^2}\frac{\partial^2 u_r}{\partial \theta^2} - 2c_{11}\frac{1}{r^2}\frac{\partial u_\theta}{\partial \theta} + c_{44}\frac{\partial^2 u_r}{\partial z^2} + \frac{(c_{11}+c_{12})}{2}\left(\frac{1}{r}\frac{\partial^2 u_r}{\partial r\partial \theta} + \frac{1}{r^2}\frac{\partial u_\theta}{\partial \theta}\right) + (c_{13}+c_{44})\frac{\partial^2 u_z}{\partial r\partial z} + \rho_s\omega^2 u_r = 0,$$

$$c_{66}\left(\frac{\partial^2 u_\theta}{\partial r^2} + \frac{1}{r}\frac{\partial u_\theta}{\partial r} - \frac{u_\theta}{r^2}\right) + c_{11}\frac{1}{r^2}\frac{\partial^2 u_\theta}{\partial \theta^2} + c_{44}\frac{\partial^2 u_\theta}{\partial z^2} + 2c_{11}\frac{1}{r^2}\frac{\partial u_r}{\partial \theta} + \frac{(c_{11}+c_{12})}{2}\left(\frac{1}{r}\frac{\partial^2 u_r}{\partial r\partial \theta} - \frac{1}{r^2}\frac{\partial u_r}{\partial \theta}\right) + (c_{13}+c_{44})\frac{1}{r}\frac{\partial^2 u_z}{\partial \theta\partial z} + \rho_s\omega^2 u_\theta = 0,$$

$$c_{44}\left(\frac{\partial^2 u_z}{\partial r^2} + \frac{1}{r}\frac{\partial u_z}{\partial r} + \frac{1}{r^2}\frac{\partial^2 u_z}{\partial \theta^2}\right) + c_{33}\frac{\partial^2 u_z}{\partial z^2} + (c_{13}+c_{44})\left(\frac{\partial^2 u_r}{\partial r\partial z} + \frac{1}{r}\frac{\partial u_r}{\partial z} + \frac{1}{r}\frac{\partial^2 u_\theta}{\partial \theta\partial z}\right) + \rho_s\omega^2 u_z = 0, \qquad (1)$$

where c_{ij} are the components of the elastic modulus tensor in Voigt recipe form, ρ_s is the solid density and the time factor $\exp(\mathrm{i}\omega t)$ is suppressed. Following Rahimian *et al.* (2007) and Khojasteh *et al.* (2008a,b,c) two potential functions, F and χ introduced by Eskandari-Ghadi (2005), are applied to handle these equations. They are related to displacement components, u_r, u_θ and u_z as follows:

$$u_r(r, \theta, z) = -\alpha_3\frac{\partial^2 F(r, \theta, z)}{\partial r\partial z} - \frac{1}{r}\frac{\partial \chi(r, \theta, z)}{\partial \theta},$$

$$u_\theta(r, \theta, z) = -\alpha_3\frac{1}{r}\frac{\partial^2 F(r, \theta, z)}{\partial \theta\partial z} + \frac{\partial \chi(r, \theta, z)}{\partial r},$$

$$u_z(r, \theta, z) = \left[(1+\alpha_1)\nabla^2_{r\theta} + \alpha_2\frac{\partial^2}{\partial z^2} + \frac{\rho_s\omega^2}{c_{66}}\right]F(r, \theta, z),$$

$$\alpha_1 = \frac{c_{12}+c_{66}}{c_{66}}, \qquad \alpha_2 = \frac{c_{44}}{c_{66}}, \qquad \alpha_3 = \frac{c_{13}+c_{44}}{c_{66}}. \qquad (2)$$

Substituting these equations into eq. (1) and applying the Hankel transform of the mth order in the radial direction and the Fourier series expansion in the angular direction, one may rewrite the partial differential equations for the potential functions in the Hankel domain as, (Rahimian *et al.* 2007)

$$\left(\tilde{\nabla}^2_{1m}\tilde{\nabla}^2_{2m} + \delta\omega^2\frac{d^2}{dz^2}\right)\tilde{F}^m_m(z) = 0,$$

$$\tilde{\nabla}^2_{0m}\tilde{\chi}^m_m = 0, \qquad (3)$$

where

$$\tilde{\nabla}^2_{im} = \frac{\rho_s\omega^2}{\mu_i c_{66}} - \xi^2 + \frac{1}{s_i^2}\frac{d^2}{dz^2}, i = 0, 1, 2. \qquad (4)$$

Here s_1 and s_2 are the roots of the strain energy function and $s_0 = 1/\alpha_2$, the quantity ξ is the Hankel transform variable, $\mu_0 = 1$, $\mu_1 = \alpha_2$, $\mu_2 = 1+\alpha_1$ and the quantity δ is given by:

$$\frac{\delta}{\rho_s} = \frac{-1}{c_{44}s_2^2} - \frac{1}{c_{11}s_1^2} + \frac{1}{c_{11}}\left(1+\frac{c_{33}}{c_{44}}\right). \qquad (5)$$

Note that (F, χ) and $(\tilde{F}^m_m, \tilde{\chi}^m_m)$ are related to each other by means of the Hankel transform and Fourier series expansion; that is,

$$[F(r, \theta, z), \chi(r, \theta, z)] = \sum_{-\infty}^{\infty}[F_m(r, z), \chi_m(r, z)]\mathrm{e}^{\mathrm{i}m\theta}, \qquad (6)$$

$$[F_m(r), \chi_m(r)] = \int_0^\infty [\tilde{F}^m_m(\xi), \tilde{\chi}^m_m(\xi)]\xi J_m(\xi r)d\xi, \qquad (7)$$

General solutions for eq. (3) are

$$\tilde{F}^m_m(\xi, z) = A_m(\xi)\mathrm{e}^{\lambda_1 z} + B_m(\xi)\mathrm{e}^{-\lambda_1 z} + C_m(\xi)\mathrm{e}^{\lambda_2 z} + D_m(\xi)\mathrm{e}^{-\lambda_2 z},$$

$$\tilde{\chi}^m_m(\xi, z) = E_m(\xi)\mathrm{e}^{\lambda_3 z} + F_m(\xi)\mathrm{e}^{-\lambda_3 z}, \qquad (8)$$

where

$$\lambda_1 = \sqrt{a\xi^2 + b + \frac{1}{2}\sqrt{c\xi^4 + d\xi^2 + e}},$$

$$\lambda_2 = \sqrt{a\xi^2 + b - \frac{1}{2}\sqrt{c\xi^4 + d\xi^2 + e}},$$

$$\lambda_3 = s_0\sqrt{\xi^2 - \frac{\rho_s\omega^2}{c_{66}}}. \qquad (9)$$

In the above,

$$a = \frac{1}{2}\left(s_1^2 + s_2^2\right),$$

$$b = -\frac{1}{2}\rho_s\omega^2\left(\frac{1}{c_{33}} + \frac{1}{c_{44}}\right),$$

$$c = \left(s_2^2 - s_1^2\right)^2,$$

$$d = -2\rho_s\omega^2\left[\left(\frac{1}{c_{33}} + \frac{1}{c_{44}}\right)\left(s_1^2 + s_2^2\right) - 2\frac{c_{11}}{c_{33}}\left(\frac{1}{c_{11}} + \frac{1}{c_{44}}\right)\right],$$

$$e = \rho_s^2\omega^4\left(\frac{1}{c_{33}} - \frac{1}{c_{44}}\right)^2. \tag{10}$$

The unknown functions A_m, B_m, C_m, D_m, E_m and F_m can be determined from the boundary conditions. Quantities λ_1, λ_2, λ_3 are multi-valued functions and are made single-valued by specifying the branch cuts emanating from the branch points $\xi_{\lambda_1} = \pm\omega\sqrt{\rho_s/c_{11}}$, $\xi_{\lambda_2} = \pm\omega\sqrt{\rho_s/c_{44}}$, $\xi_{\lambda_3} = \pm\omega\sqrt{\rho_s/c_{66}}$ in the complex ξ-plane, such that the real parts of λ_1, λ_2, λ_3 are non-negative for all values of ξ (Rahimian *et al.* 2007). The positive sign of these branch points denotes the wavenumbers of the body waves, P, SV and SH, respectively.

The equations for the transformed stress and displacement components obtained by eq. (2) and Hankel transform identities, which will be necessary in applying the boundary conditions pertaining to the normal and tangential components of stress and displacement at the interfaces are:

$$\tilde{u}_{z_m}^m = \left[\alpha_2\frac{d^2}{dz^2} + \frac{\rho_s\omega^2}{c_{66}} - \xi^2(1+\alpha_1)\right]\tilde{F}_m^m,$$

$$\tilde{u}_{r_m}^{m+1} + i\tilde{u}_{\theta_m}^{m+1} = \alpha_3\xi\frac{d\tilde{F}_m^m}{dz} - i\xi\tilde{\chi}_m^m,$$

$$\tilde{u}_{r_m}^{m-1} - i\tilde{u}_{\theta_m}^{m-1} = -\alpha_3\xi\frac{d\tilde{F}_m^m}{dz} - i\xi\tilde{\chi}_m^m,$$

$$\tilde{\sigma}_{zz_m}^m = \frac{d}{dz}\left[\alpha_3 c_{13}\xi^2 + c_{33}\left(\frac{\rho_s\omega^2}{c_{66}} - \xi^2(1+\alpha_1)\right) + c_{33}\alpha_2\frac{d^2}{dz^2}\right]\tilde{F}_m^m,$$

$$\tilde{\sigma}_{zr_m}^{m+1} + i\tilde{\sigma}_{z\theta_m}^{m+1} = c_{44}\xi\left[(\alpha_3 - \alpha_2)\frac{d^2}{dz^2} + \xi^2(1+\alpha_1) - \frac{\rho_s\omega^2}{c_{66}}\right]\tilde{F}_m^m - c_{44}\xi i\frac{d\tilde{\chi}_m^m}{dz},$$

$$\tilde{\sigma}_{zr_m}^{m-1} - i\tilde{\sigma}_{z\theta_m}^{m-1} = -c_{44}\xi\left[(\alpha_3 - \alpha_2)\frac{d^2}{dz^2} + \xi^2(1+\alpha_1) - \frac{\rho_s\omega^2}{c_{66}}\right]\tilde{F}_m^m - c_{44}\xi i\frac{d\tilde{\chi}_m^m}{dz}. \tag{11}$$

The formulations expressed above are valid for a general transversely isotropic solid having a vertical axis of symmetry. Hereafter, the variables which are associated with the middle layer and the bottom half-space are indicated by superscripts II and III, respectively.

For the liquid layer, deemed to be a light one such as water, the governing equation of motion in a cylindrical coordinate system is given by (Ewing *et al.* 1957):

$$\frac{\partial^2\varphi}{\partial t^2} = c_l^2\nabla^2\varphi(r, \theta, z), \tag{12}$$

where $c_l = \sqrt{K/\rho_l}$ is the velocity of the dilatational wave in the liquid and φ is the displacement potential. K and ρ_l are the bulk modulus and density of the liquid, respectively. The displacement components and the pressure can be expressed in terms of φ as:

$$u_r = \frac{\partial\varphi}{\partial r}, \quad u_z = \frac{\partial\varphi}{\partial z},$$

$$P = K\frac{\omega^2}{c_l^2}\varphi, \tag{13}$$

where harmonic time dependence $\exp(i\omega t)$ is assumed (or equivalently we are dealing with the pressure and displacement spectra).

Applying the Fourier series expansion with respect to the angular coordinate and the mth order Hankel transform with respect to the radial coordinate one may obtain the following equation for the liquid layer,

$$\tilde{\nabla}_{0m}^2\tilde{\varphi}_m^m = 0. \tag{14}$$

A general solution of this equation is

$$\tilde{\varphi}_m^m = S_m(\xi)e^{-\lambda_4 z} + R_m(\xi)e^{\lambda_4 z}, \tag{15}$$

where

$$\lambda_4 = \sqrt{\xi^2 - \frac{\omega^2}{c_l^2}}. \tag{16}$$

$c_l = \sqrt{K/\rho_l}$ is the velocity of the dilatational wave in the liquid. The unknown functions S_m and R_m will be determined through the boundary conditions of continuity of normal components of stress and displacement, where according to sign selection, R_m and S_m are the transformed amplitude functions of the transmitted and reflected waves.

The stress and displacement components in the Fourier domain for the transformed mode are written as

$$\tilde{\sigma}_{zz_m}^m = -\tilde{P} = -\rho_l \omega^2 \tilde{\varphi}_m^m,$$

$$\tilde{u}_{z_m}^m = \frac{\partial \tilde{\varphi}_m^m}{\partial z}. \tag{17}$$

3 BOUNDARY CONDITIONS AND FREQUENCY EQUATION

The boundary conditions are imposed to obtain the frequency equation. According to the Sommerfeld radiation condition, the coefficients A_m^{III}, C_m^{III}, E_m^{III} vanish. The boundary conditions at the free surface and at the two interfaces will now be applied. The free-surface condition (at $z = 0$) implies that

$$S_m(\xi) = -R_m(\xi). \tag{18}$$

Hence, one can rewrite the potential function of the liquid subdomain as

$$\tilde{\varphi}_m^m = S_m(\xi) \sinh(\lambda_4 z). \tag{19}$$

Thus, one of the unknown functions is suppressed. Note that S_m now differs from the previous definition by a constant multiplying factor. At the liquid–solid interface ($z = h$) the boundary conditions include the normal stress and displacement continuity where according to the inviscid liquid assumption, the shear stress components of the solid domain vanish at the interface. Hence, at $z = h$, one may write

$$\sigma_{zz_m}^{m^I}(z = h^-) = \sigma_{zz_m}^{m^{II}}(z = h^+),$$

$$u_{z_m}^{m^I}(z = h^-) = u_{z_m}^{m^{II}}(z = h^+),$$

$$\tilde{\sigma}_{zr_m}^{m+1^{II}}(z = h^+) + i\tilde{\sigma}_{z\theta_m}^{m+1^{II}}(z = h^+) = 0,$$

$$\tilde{\sigma}_{zr_m}^{m-1^{II}}(z = h^+) - i\tilde{\sigma}_{z\theta_m}^{m-1^{II}}(z = h^+) = 0. \tag{20}$$

At the interface between the solid layer and the underlying solid half-space, $z = H$ where $H = h + h'$, the continuity of all the displacement and stress components should be maintained, that is,

$$\sigma_{zz_m}^{m^{II}}(z = H^-) = \sigma_{zz_m}^{m^{III}}(z = H^+),$$

$$\tilde{\sigma}_{zr_m}^{m+1^{II}}(z = H^-) + i\tilde{\sigma}_{z\theta_m}^{m+1^{II}}(z = H^-) = \tilde{\sigma}_{zr_m}^{m+1^{III}}(z = H^+) + i\tilde{\sigma}_{z\theta_m}^{m+1^{III}}(z = H^+),$$

$$\tilde{\sigma}_{zr_m}^{m-1^{II}}(z = H^-) - i\tilde{\sigma}_{z\theta_m}^{m-1^{II}}(z = H^-) = \tilde{\sigma}_{zr_m}^{m-1^{III}}(z = H^+) - i\tilde{\sigma}_{z\theta_m}^{m-1^{III}}(z = H^+),$$

$$u_{z_m}^{m^{II}}(z = H^-) = u_{z_m}^{m^{III}}(z = H^+),$$

$$\tilde{u}_{r_m}^{m+1^{II}}(z = H^-) + i\tilde{u}_{\theta_m}^{m+1^{II}}(z = H^-) = \tilde{u}_{r_m}^{m+1^{III}}(z = H^+) + i\tilde{u}_{\theta_m}^{m+1^{III}}(z = H^+),$$

$$\tilde{u}_{r_m}^{m-1^{II}}(z = H^-) - i\tilde{u}_{\theta_m}^{m-1^{II}}(z = H^-) = \tilde{u}_{r_m}^{m-1^{III}}(z = H^+) - i\tilde{u}_{\theta_m}^{m-1^{III}}(z = H^+). \tag{21}$$

Ten equations are obtained for the ten unknown functions which form a 10th-order system of equations. By utilizing eq. (11) one can obtain the frequency equation of the surface waves by letting the determinant of the matrix go to zero. However, the matrix equation can be divided into two separate sets of rows for two sets of unknown functions which are independent from each other. One expresses the frequency equation for the Love wave and the other one is independently associated with the rest of the possible waves (Rayleigh, Scholte and Stoneley).
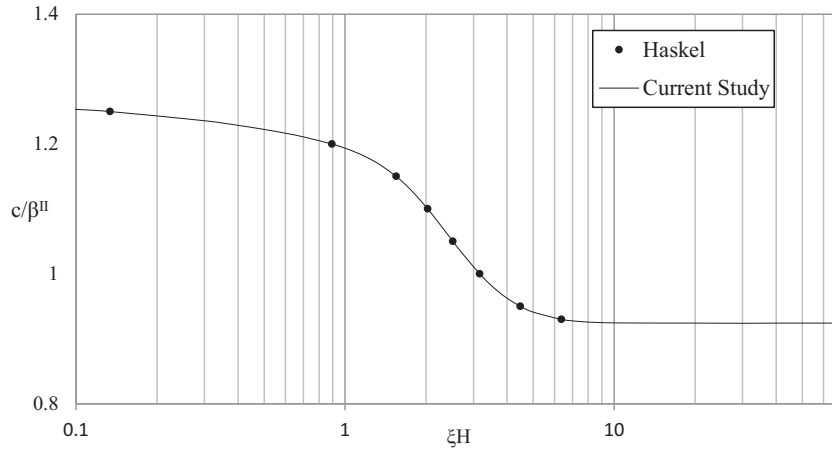
Figure 2. Rayleigh and Stoneley (Scholte) wave phase velocity dispersion curve for an isotropic solid layer overlying an elastic solid half-space, $\rho_s^{III}/\rho_s^{II} = 1.11$, $\beta^{III}/\beta^{II} = 1.37$, $\alpha^{III}/\beta^{II} = 2.44$, $\alpha^{II}/\beta^{II} = 1.81$.
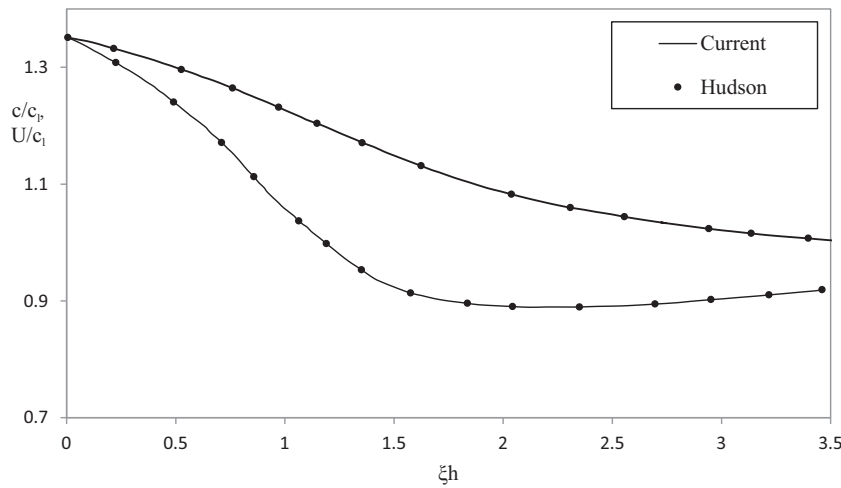

Figure 3. Rayleigh and Stoneley (Scholte) wave phase and group velocity dispersion curves for a liquid layer overlying transversely isotropic half-space.

For the latter the equations can be expressed in the determinant form as follows:

$$
\begin{vmatrix}
\lambda_4 \cosh \lambda_4 h & -\vartheta_1^{II} e^{\lambda_1^{II} h} & -\vartheta_1^{II} e^{-\lambda_1^{II} h} & -\vartheta_2^{II} e^{\lambda_2^{II} h} & -\vartheta_2^{II} e^{-\lambda_2^{II} h} & 0 & 0 \\
-\rho_l \omega^2 \sinh \lambda_4 h & c_{33}^{II} e^{\lambda_1^{II} h} v_1^{II} & -c_{33}^{II} e^{-\lambda_1^{II} h} v_1^{II} & c_{33}^{II} e^{\lambda_2^{II} h} v_2^{II} & -c_{33}^{II} e^{-\lambda_2^{II} h} v_2^{II} & 0 & 0 \\
0 & -c_{44}^{II} e^{\lambda_1^{II} h} \eta_1^{II} & -c_{44}^{II} e^{-\lambda_1^{II} h} \eta_1^{II} & -c_{44}^{II} e^{\lambda_2^{II} h} \eta_2^{II} & -c_{44}^{II} e^{-\lambda_2^{II} h} \eta_2^{II} & 0 & 0 \\
0 & \alpha_3^{II} \lambda_1^{II} e^{\lambda_1^{II} H} & -\alpha_3^{II} \lambda_1^{II} e^{-\lambda_1^{II} H} & \alpha_3^{II} \lambda_2^{II} e^{\lambda_2^{II} H} & -\alpha_3^{II} \lambda_2^{II} e^{-\lambda_2^{II} H} & \alpha_3^{III} \lambda_1^{III} e^{-\lambda_1^{III} H} & \alpha_3^{III} \lambda_2^{III} e^{-\lambda_2^{III} H} \\
0 & \vartheta_1^{II} e^{\lambda_1^{II} H} & \vartheta_1^{II} e^{-\lambda_1^{II} H} & \vartheta_1^{II} e^{\lambda_2^{II} H} & \vartheta_1^{II} e^{-\lambda_2^{II} H} & -\vartheta_1^{III} e^{-\lambda_1^{III} H} & -\vartheta_2^{III} e^{-\lambda_2^{III} H} \\
0 & c_{44}^{II} e^{\lambda_1^{II} H} \eta_1^{II} & c_{44}^{II} e^{-\lambda_1^{II} H} \eta_1^{II} & c_{44}^{II} e^{\lambda_2^{II} H} \eta_2^{II} & c_{44}^{II} e^{-\lambda_2^{II} H} \eta_2^{II} & -c_{44}^{III} \eta_1^{III} e^{-\lambda_1^{III} H} & -c_{44}^{III} \eta_2^{III} e^{-\lambda_2^{III} H} \\
0 & -c_{33}^{II} v_1^{II} e^{\lambda_1^{II} H} & c_{33}^{II} v_1^{II} e^{-\lambda_1^{II} H} & -c_{33}^{II} v_2^{II} e^{\lambda_2^{II} H} & c_{33}^{II} v_2^{II} e^{-\lambda_2^{II} H} & -c_{33}^{III} \eta_1^{III} e^{-\lambda_1^{III} H} & -c_{33}^{III} \eta_2^{III} e^{-\lambda_2^{III} H}
\end{vmatrix} = 0 \quad (22)
$$

Eq. (22) is associated with the unknown function vector $[S_m, A_m^{II}, B_m^{II}, C_m^{II}, D_m^{II}, B_m^{III}, D_m^{III}]^T$ and includes terms of λ_1, λ_2 and λ_4. For the Love wave the equations can be expressed as

$$
\begin{vmatrix}
-i\lambda_3^{II} c_{44}^{II} e^{\lambda_3^{II} h} & i\lambda_3^{II} c_{44}^{II} e^{-\lambda_3^{II} h} & 0 \\
e^{\lambda_3^{II} H} & e^{-\lambda_3^{II} H} & -e^{-\lambda_3^{III} H} \\
-ic_{44}^{II} \lambda_3^{II} e^{\lambda_3^{II} H} & ic_{44}^{II} \lambda_3^{II} e^{-\lambda_3^{II} H} & -ic_{44}^{III} \lambda_3^{III} e^{-\lambda_3^{III} H}
\end{vmatrix} = 0. \quad (23)
$$

Eq. (23) is associated with the unknown function vector $[E_m^{II}, F_m^{II}, F_m^{III}]^T$ and includes terms of λ_3.

Table 1. Material properties, Poulos & Davis (1974) and Khojasteh *et al.* (2008c, 2013).

Material	ρ (kg m^{-3})	c_{44} (GPa)	c_{11} (GPa)	c_{12} (GPa)	c_{13} (GPa)	c_{33} (GPa)
1	2500	10	41.3	14.7	10.1	36.2
2	5000	50	553	280	250	250
3	900	9	47.9	15.9	11.2	23.9
4	2500	10	27.2	7.2	8.6	129.9

Table 2. Model properties.

Model number	Liquid layer (I)	VTI solid layer (II)	VTI solid half-space (III)
1	Water	Material 1	Material 2
2	Water	Material 2	Material 3
3	Water	Material 4	Material 2
4	Water	Material 1	Material 4

In the above equations, we have made the following abbreviations:

$$\eta_i = (\alpha_3 - \alpha_2)\lambda_i^2 + \xi^2(1 + \alpha_1) - \frac{\rho_s \omega^2}{c_{66}}, \quad \vartheta_i = \alpha_3 \lambda_i^2 - \eta_i,$$

$$\nu_i = \left(\eta_i - \alpha_3 \frac{c_{13}}{c_{33}} \xi^2 - \alpha_3 \lambda_i^2 \right) \lambda_i, i = 1, 2. \tag{24}$$

There is no appearance of the liquid layer in the Love wave equation, that is, the inviscid liquid layer has no effect here. Hence, this equation is the same as that for the case a transversely isotropic solid overlying a transversely isotropic half-space as is given in (Khojasteh *et al.* 2008c). Nevertheless, we are still interested in presenting dispersion curves for Love waves, because there is no illustration and interpretation of these curves in the references for such a model.
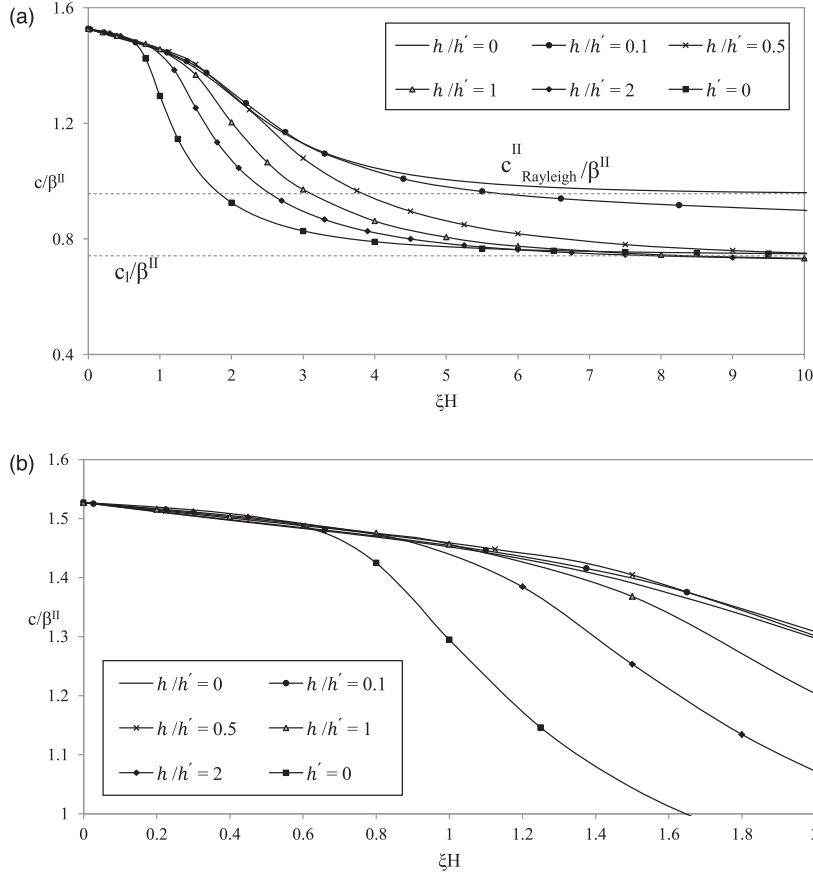
Figure 4. (a) Rayleigh and Stoneley (Scholte) wave phase velocity dispersion curves for six values of the layer thickness ratios in Model 1. (b) Zoomed-in version of Rayleigh and Stoneley (Scholte) wave phase velocity curves at low dimensionless wavenumbers in Model 1.
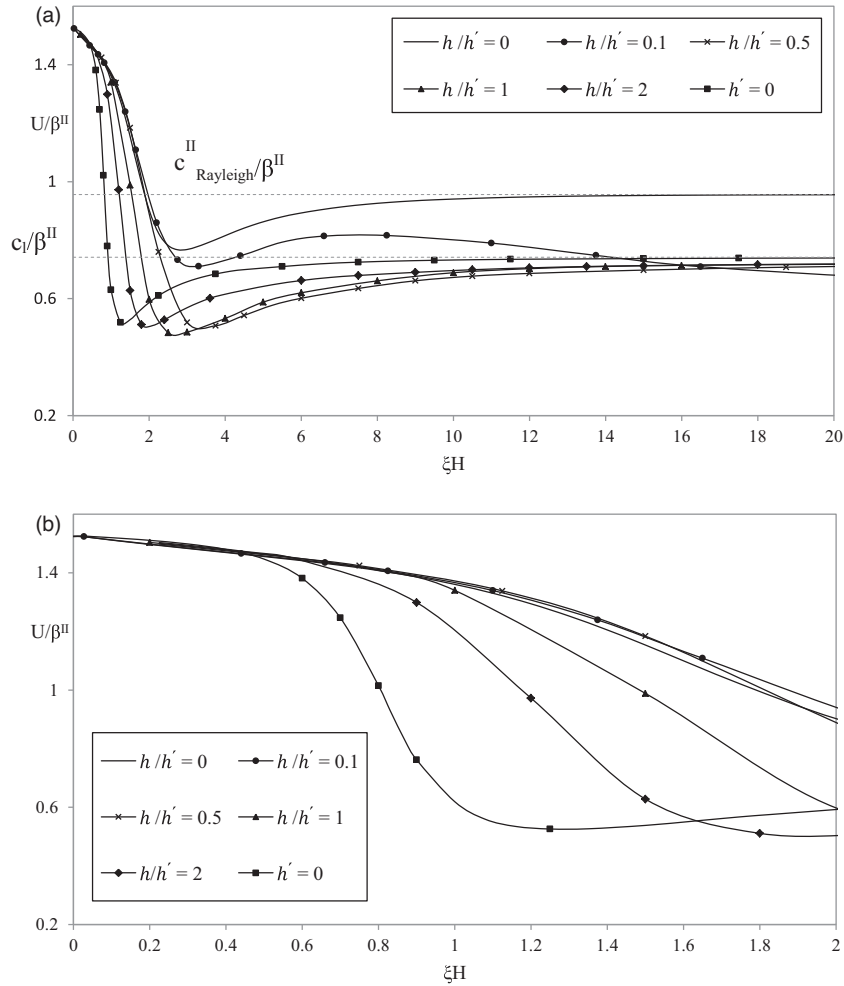
Figure 5. (a) Rayleigh and Stoneley (Scholte) wave group velocity dispersion of curves for six values of layer thickness ratios in Model 1. (b) Zoomed-in version of Rayleigh and Stoneley (Scholte) wave group velocity of dispersion at low dimensionless wavenumbers in Model 1.

Solving the frequency eq. (22)—made up of potential functions $\tilde{F}_m^{II}$, $\tilde{F}_m^{III}$ and $\tilde{\varphi}_m$—and (23)—made up of potential functions $\tilde{\chi}_m^{II}$ and $\tilde{\chi}_m^{III}$—provides us with the dispersion curves of waves of different types. Eq. (22) is used to derive the generalized Rayleigh and Scholte waves at the liquid–solid interface and also the Stoneley waves at the solid–solid interface. The appearance of a Stoneley wave for the solid–solid interface requires stringent conditions including specific elastic properties of the two solids and the depths of the layers. In general, when the velocities of the SV waves of two solids are close to each other (Ewing *et al.* 1957) and the depth of the overlying layer increases, there is a higher probability of appearance for this kind of interface wave. A discussion about the conditions required for occurrence of such waves is given by Barnett (2000) and Kuznetsov (2006) and the reader is referred to these papers for a thorough analysis. The largest values of the roots of eqs (22) and (23) denote the wavenumber associated with the first or fundamental mode and the Love wavenumber, respectively. Smaller roots for a given frequency ω may arise as the value of ξh increases and are associated with the higher modes of generalized Rayleigh and Love waves propagating with a higher phase velocity than that of the first mode. However, in the Rayleigh wave frequency equation only the first modes include the Stoneley or Scholte branch. In the sequence of the frequency root values, the root with respect to the Scholte wave falls immediately before the frequency of the compressional wave in the liquid.

The general shape of the Rayleigh wave dispersion curves may differ according to the body wave velocities and densities of the two materials. More discussion on this topic is given in Section 5.

4 SPECIAL CASES

Several special cases can be considered and simpler problems can be extracted from the more general results.

Case 1. The Scholte (or also referred to as the Stoneley) wave frequency equation can be obtained by letting ξh and ξH values tend to infinity in eq. (22), that is, the liquid and the middle layer thicknesses take on large values in comparison to the wavelength (proportional to $1/\xi$). The root of the frequency equation is pertinent to the wavenumber of the interface wave associated with the Scholte wave for a liquid layer overlying a half-space, which consists of the middle layer material, regardless of the lowermost layer. For the Scholte wave the frequency
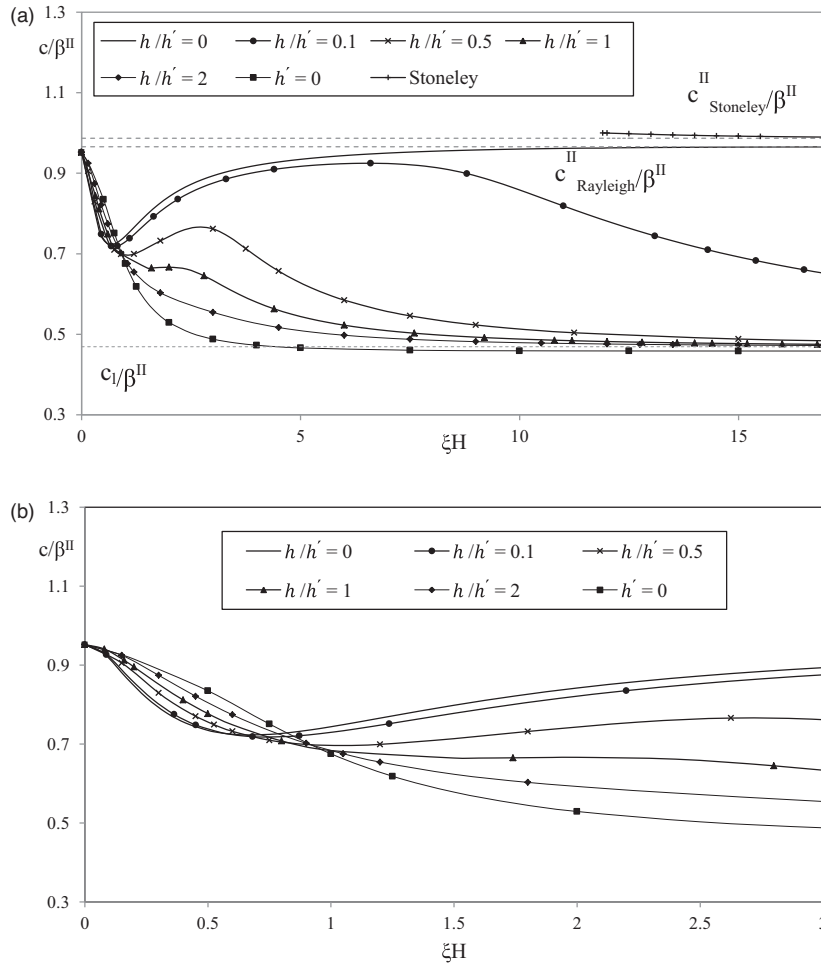
Figure 6. (a) Rayleigh and Stoneley (Scholte) wave phase velocity dispersion curves for six values of layer thickness ratios in Model 2. (b) Zoomed-in version of Rayleigh and Stoneley (Scholte) wave phase velocity curves at low dimensionless wavenumbers in Model 2.

equation reduces to the following which is the same equation obtained by Abubakar & Hudson (1961) for a model of a liquid layer overlying a transversely isotropic half-space:

$$\rho_l \omega^2 \left(\eta_2^{II} \vartheta_1^{II} - \eta_1^{II} \vartheta_2^{II} \right) + \lambda_4 \left(\eta_2^{II} v_1^{II} - \eta_1^{II} v_2^{II} \right) = 0. \tag{25}$$

Moreover, the wavenumber of the Stoneley wave, if it exists, at the solid–solid interface arises as another root. It is given by:

$$
\begin{aligned}
\alpha_3^{III} &\left[c_{44}^{III} \left(\vartheta_1^{II} v_2^{II} - \vartheta_2^{II} v_1^{II} \right) \left(\eta_1^{III} \lambda_2^{III} - \eta_2^{III} \lambda_1^{III} \right) + c_{44}^{II} \left(\eta_2^{II} v_1^{II} - \eta_1^{II} v_2^{II} \right) \left(\lambda_2^{III} \vartheta_1^{III} - \lambda_1^{III} \vartheta_2^{III} \right) \right. \\
&\left. + c_{44}^{II} \left(\eta_2^{II} \vartheta_1^{II} - \eta_1^{II} \vartheta_2^{II} \right) \left(\lambda_2^{III} v_1^{III} - \lambda_1^{III} v_2^{III} \right) \right] \\
&+ \alpha_3^{II} \left[c_{44}^{III} \left(\vartheta_1^{III} v_2^{III} - \vartheta_2^{III} v_1^{III} \right) \left(\eta_1^{II} \lambda_2^{II} - \eta_2^{II} \lambda_1^{II} \right) + c_{44}^{III} \left(\eta_2^{II} v_1^{III} - \eta_1^{III} v_2^{III} \right) \left(\lambda_2^{II} \vartheta_1^{II} - \lambda_1^{II} \vartheta_2^{II} \right) \right. \\
&\left. + c_{44}^{III} \left(\eta_2^{III} \vartheta_1^{III} - \eta_1^{III} \vartheta_2^{III} \right) \left(\lambda_2^{II} v_1^{II} - \lambda_1^{II} v_2^{II} \right) \right] = 0,
\end{aligned}
\tag{26}
$$

This is the equation derived by Khojasteh *et al.* (2008b)

Case 2. At the long wavelength limit, that is ξH tending to zero, the first frequency eq. (22) reduces to that of a Rayleigh wave for a transversely isotropic solid half-space, that is $\eta_1^{III} v_2^{III} - \eta_2^{III} v_1^{III} = 0$. By substituting the elastic constants of an isotropic solid, that is setting $c_{11} = c_{33} = \lambda + 2\mu$, $c_{12} = c_{13} = \lambda$, $c_{44} = c_{66} = \mu$, the well-known Rayleigh wave cubic equation for an isotropic elastic half-space can also be obtained.

Case 3. When h' tends to zero, or the elastic constants and density of the middle layer are put equal to those of the lowermost material, we obtain from the general result the dispersion of surface waves for a liquid layer overlying a half-space consisting of the bottom material. The frequency equation in this case leads to the following which is identical to the equation obtained by Abubakar & Hudson (1961):

$$c_{33}^{III} \lambda_4 \left(\eta_2^{III} v_1^{III} - \eta_1^{III} v_2^{III} \right) \operatorname{Cosh}(\lambda_4 h) + \rho_l \omega^2 \left(\eta_2^{III} \vartheta_1^{III} - \eta_1^{III} \vartheta_2^{III} \right) \operatorname{Sinh}(\lambda_4 h) = 0. \tag{27}$$

Case 4. If h vanishes (i.e. the liquid layer is removed), the equations yield those of a transversely isotropic layer overlying a half-space which is made up of a contrasting transversely isotropic material (Ewing *et al.* 1957).
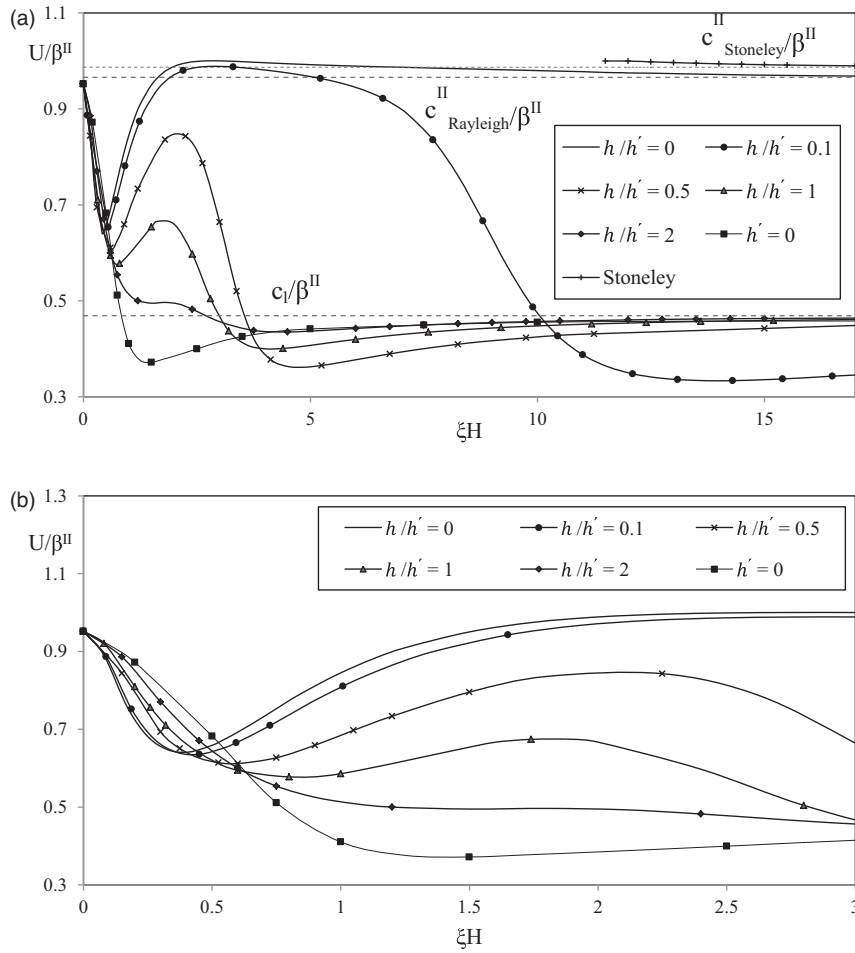
Figure 7. (a) Rayleigh and Stoneley (Scholte) wave group velocity curves for six values of layer thicknesses ratios in Model 2. (b) Zoomed-in version of Rayleigh and Stoneley (Scholte) wave group velocity dispersion for low dimensionless wavenumbers in Model 2.

Case 5. If the solid materials are considered to be isotropic, the wavenumbers associated with the body waves in the solid become $\xi_p = \omega\sqrt{\rho_s/(2\mu + \lambda)}$ and $\xi_{SH} = \xi_{SV} = \omega\sqrt{\rho_s/\mu}$, and the two frequency equations reduce to the Rayleigh and Love wave equations developed by Ewing *et al.* (1957) for a half-space made up of a liquid layer above a finite thickness isotropic solid overlying dissimilar isotropic solid basement. Also, in some cases a transversely isotropic material overlying an isotropic basement can be encountered and this case can be analysed by setting the appropriate elastic constants.

Case 6. If the thickness of the liquid layer is set to zero and the material properties of the two layers are made isotropic then one can obtain the results developed by Ewing *et al.* (1957) and Abubakar & Hudson (1961) for an isotropic solid layer overlying an isotropic solid half-space.

5   NUMERICAL RESULTS

The implicit relationship between the wavenumber ξ of the surface/interface waves and the frequency of the waves ω, that is the dispersion relation, will now be examined numerically for certain models. Curves of the dimensionless phase ($c = \omega/\xi$) and group ($U = \mathrm{d}\omega/\mathrm{d}\xi$) velocity of each type of wave can be obtained with the aid of these equations. In these figures, $\beta^{II} = \sqrt{c_{44}^{II}/\rho_s^{II}}$.

As confirmation of two special cases, a two layered solid half-space made up of two isotropic materials, studied by Haskell (1953) is first considered by appropriate choice of the elastic constants. The materials properties of the two layers yield the following density and velocity ratios: $\rho_s^{III}/\rho_s^{II} = 1.11$, $\beta^{III}/\beta^{II} = 1.37$, $\alpha^{III}/\beta^{II} = 2.44$, $\alpha^{II}/\beta^{II} = 1.81$, where α and β are the velocities of the dilatational and distortional transverse body waves in an isotropic solid, respectively. Phase velocity curves are presented in Fig. 2 which show good agreement with those presented by Haskell (1953). Fig. 3 shows the agreement of the results with those presented by Abubakar & Hudson (1961), for another special case when $h' = 0$, where the elastic properties of the liquid and the lower VTI half-space are such that $\rho_S/\rho_l = 2$, $c_{SV}/c_l = \sqrt{2}$, $c_P/c_{SV} = 2.032$.

For a more insightful assessment of dispersion characteristics, and to appreciate how the shape of the curves may differ depending on the pattern of body wave velocities and mass densities of the layers, four different configurations are selected for consideration. Four kinds
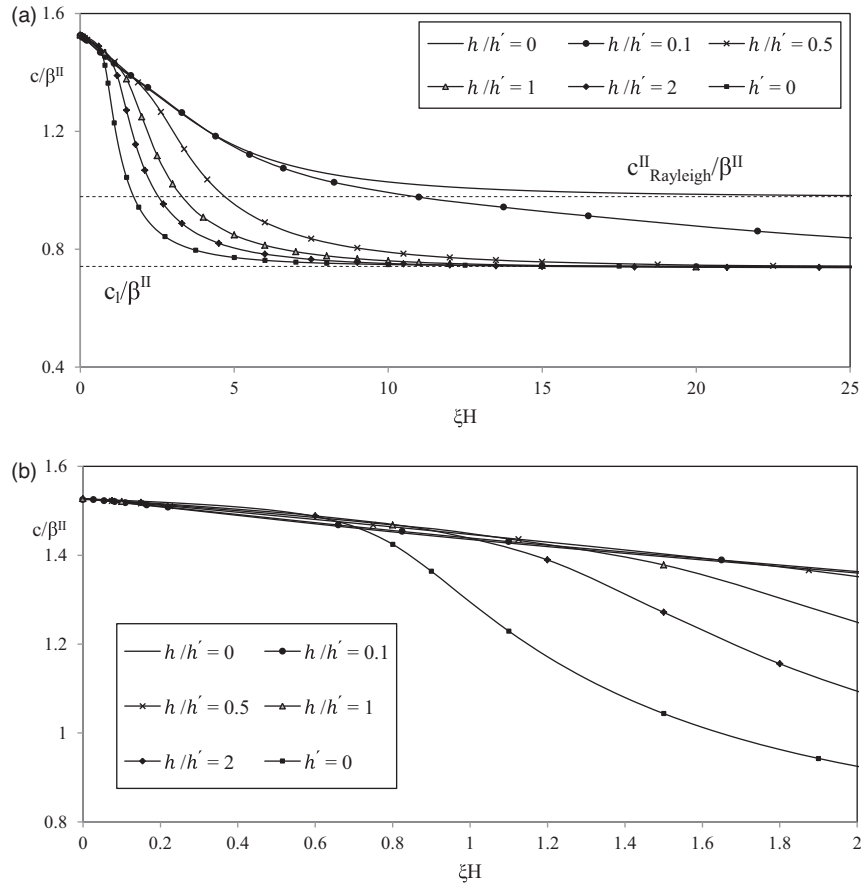
Figure 8. (a) Rayleigh and Stoneley (Scholte) wave phase velocity dispersion curves for six values of layer thicknesses ratios in Model 3. (b) Zoomed-in version of Rayleigh and Stoneley (Scholte) wave phase velocity dispersion for low dimensionless wavenumber in Model 3.

of transversely isotropic solid materials are selected following the materials used by Poulos & Davis (1974) and Khojasteh *et al.* (2008c, 2013). The elastic properties are given in Table 1. Recall that for this kind of material, $c_{12} = c_{11} - 2c_{66}$. The liquid is assumed to be water with $\rho_l = 1000$ kg m^{-3} and $K = 2.2 \times 10^9$ (GPa). The four models obtained by different combinations of the four introduced materials are listed in Table 2. Model numbers 1, 3 and 4 do not meet the necessary conditions for Stoneley wave existence, whereas model No. 2 does, for which in the dispersion of the Stoneley wave at the solid–solid interface is computed. Curves for the fundamental mode are plotted for different values of the ratio of water layer thickness to solid layer thickness h/h' in all cases. Note that the normalized values of the Rayleigh wave velocity for a half-space consisting of the middle solid layer material of each model, the compressional wave velocity in the liquid layer and the limiting value of the Stoneley wave velocity are indicated in the figures by means of the dashed lines. The solution of the frequency equations was handled by means of a computer program in Mathematica. Special care must be taken in order not to misplace the dispersion curves when dealing with the frequency equations, since for a specific dimensionless wavenumber ξ several roots may be encountered which are associated with the fundamental and higher modes. The solver should be given a suitable point in the vicinity of the desired root. To determine the fundamental mode, which is presented in the figures, the two benchmarks provided by the two extreme cases can be helpful. One can start drawing the fundamental mode by inputting a zero or adequately low value for frequency/wavenumber to find a single root which is associated with the fundamental mode. By steadily increasing the frequency/wavenumber, the fundamental mode can be drawn to large values of horizontal axis variable to yield to the Scholte branch which necessarily belongs to the fundamental mode as the second benchmark.

Figs 4–11 represent the phase and group velocity dispersion curves for surface waves in the four models. Each curve is given at two different resolutions, indicated with 'a' and 'b', respectively, to illustrate the results more clearly for the entire frequency range and for the low frequency range. In the figures, various values of h/h' are assumed (0, 0.1, 0.5, 1) along with the case $h' = 0$ ($h/h' = \infty$) and the dispersion characteristics are plotted for each situation. This includes both cases where the liquid layer thickness is greater or less than the thickness of the middle anisotropic solid layer. Also, two specific cases are considered where the middle layer thickness h' is decreased to zero, and where the water layer thickness is set to zero, that is, there is no liquid layer overlying the solid layer. Except in the case where $h = 0$, the phase velocity curve separates into two branches, at a critical value of phase velocity $c = c_l$. In the excluded case the extreme value of the velocities are those for the Rayleigh wave in a transversely isotropic half-space, made up of the middle layer material, regardless of the bottom-most material. For the rest of the curves, the velocity values greater than c_l are associated with the normal mode branch, and the lower values represent the Stoneley (Scholte) branch in a three layered media. In all these curves, the normal mode reaches the asymptotic value of the
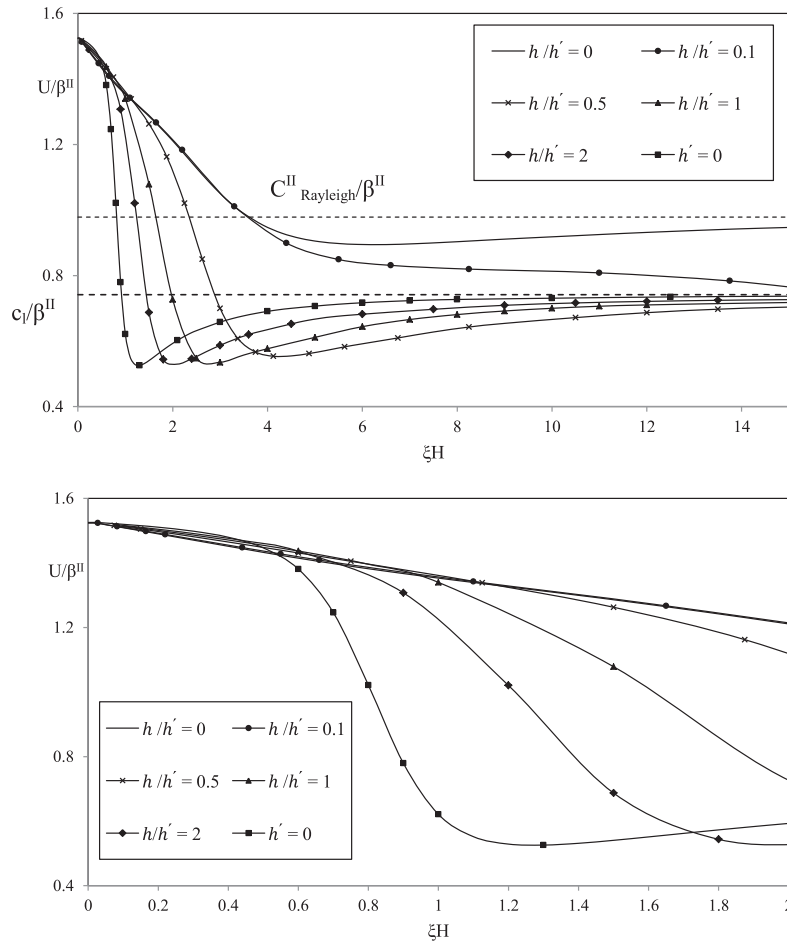
Figure 9. (a) Rayleigh and Stoneley (Scholte) wave group velocity dispersion curves for six values of layer thickness ratio in Model 3. (b) Zoomed-in version of Rayleigh and Stoneley (Scholte) wave group velocity dispersion for low dimensionless wavenumbers in Model 3.

Scholte wave in a model where the liquid layer overlies a half-space, as ξh tends to large values, except in the obvious case when $h' = 0$. All the curves in the long wave limit meet the value of the Rayleigh wave velocity at the free surface of a half-space comprising the basal material. It can be observed that the greater the value of h/h' the more rapid the trend towards the Scholte wave. Also, in the four models it is observed that as the thickness of the middle layer increases, the curves remain in the normal mode branch of propagation for a larger range of ξh values. As a consequence, a thicker liquid layer causes the Scholte branch to arise at a lower frequency. Group velocity curves are also given and show one or more maxima and/or minima.

One can examine the importance of the basal half-space by comparing results for Models No. 1 and No. 4. The liquid layer and the middle layer materials are the same in each case; the only difference is half-space elasticity and density. The effect of the middle layer can be examined comparing Models No. 1 and No. 3, which share the same water layer and half-space materials. Although the liquid layer has an effect on dispersion properties in all of the models, it seems to be more significant in Models No. 2 and No. 4. For Model No. 4, in the special case $h = 0$ (i.e. in absence of the liquid layer), one can recognize a maximum point close to $\xi H = 0.75$ (Figs 10a,b and 11a,b). But if the liquid layer is thick enough relative to the middle layer thickness, then the maximum disappears. This occurs in similar fashion for the minimum point which arises in the dispersion curve of Model No. 2 as depicted in Figs 6a,b and 7a,b. For Model No. 2, due to the specific properties of the materials, maxima and minima appear in the phase velocity dispersion curves for some values of h/h'. For this model, these extremal points disappear as the layer thickness becomes large enough.

In Model No. 2 one can also observe another branch occurring as the ξh value reaches large values; this is associated with the Stoneley wave branch and represents a wave propagating at the interface of the two solids. Given the fact that this kind of wave appearance usually requires a large value of thickness of the solid layer above the half space, the existence of the liquid layer does not have a significant effect on its velocity. The upper limit of the Stoneley wave velocity is the SV wave velocity of the layer, which is equal to $\sqrt{c_{44}/\rho_s}$. The difference between the velocities of SH and SV waves in a transversely isotropic material, unlike the isotropic case, results in a difference in the upper limit of the Stoneley and Love wave phase velocities. The upper limit of the Love wave phase velocity for the solid–solid configuration is the value of the SH wave velocity of the bottom material, whereas this limit is the SV wave velocity for the Stoneley wave branch. The Stoneley wave branch reaches its asymptotic value very rapidly as the value of ξh increases.
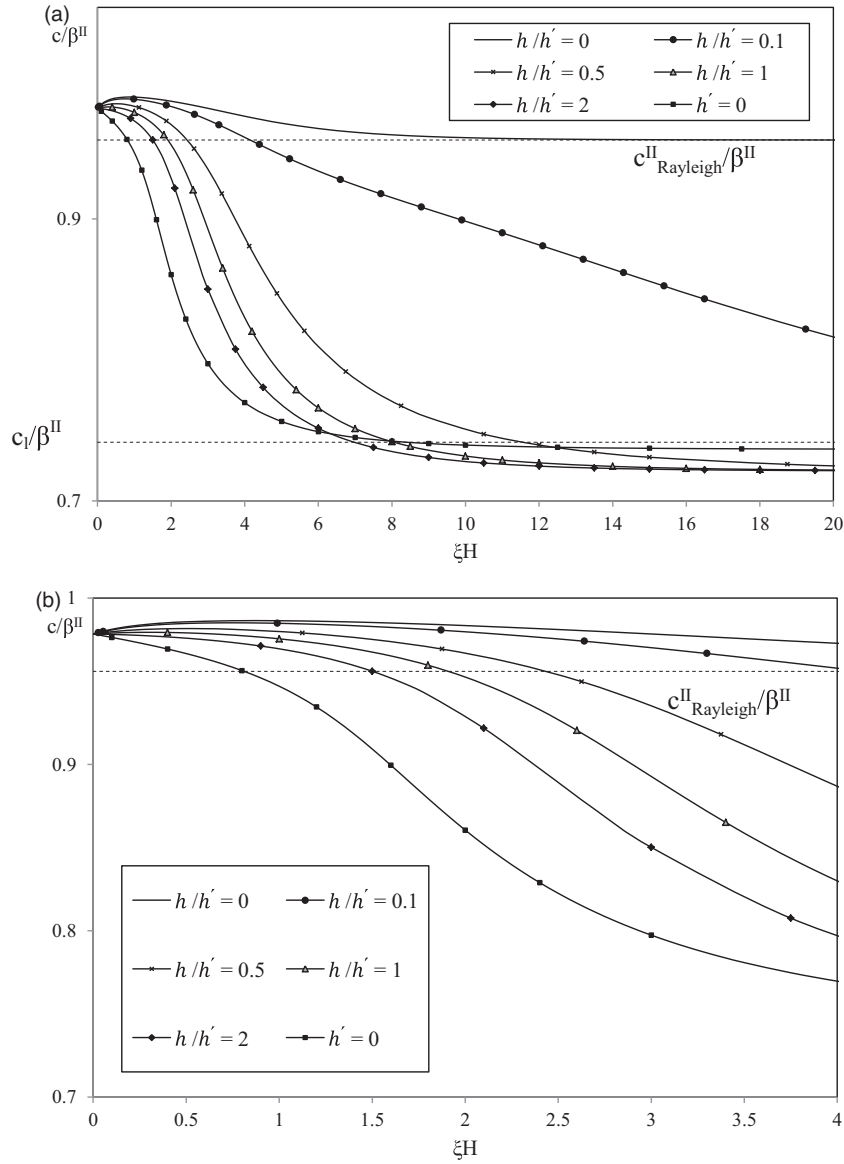
Figure 10. (a) Rayleigh and Stoneley (Scholte) wave phase velocity dispersion curves for six values of layer thickness ratios in Model 4. (b) Zoomed-in version of Rayleigh and Stoneley (Scholte) wave phase velocity dispersion for low dimensionless wavenumbers in Model 4.

Love wave dispersion curves for Model No. 1 and No. 3 are presented in Figs 12 and 13. However, in the case of Models No. 2 and No. 4, the shear wave velocity of the lower medium is not greater than that of the upper medium, and so these models do not meet the necessary conditions for the existence of Love waves. The phase velocity curves lie between the SH wave velocities of the two materials, that is $\sqrt{c_{66}^{III}/\rho_s^{III}}$ and $\sqrt{c_{66}^{II}/\rho_s^{II}}$ and smoothly decrease with increasing wavenumber (or frequency). The group velocity dispersion curve exhibits a well-defined minimum or Airy phase.

To examine the effect of anisotropy of the bottom half-space we can start with the E, E', ν and ν' values called the engineering constants-where E and E' are the Young's moduli with respect to directions lying in the plane of isotropy and perpendicular to it; ν is the Poison's ratio which characterizes the effect of horizontal strain on the complementary vertical strain; ν' is the Poisson's ratio which characterizes the effect of vertical strain on the horizontal one. For the VTI half-space in Model 1 (Material 2) with the elastic properties listed in Table 1, these constants are $E = 300$ GPa, $E' = 100$ GPa, $\nu = 0.1$ and $\nu' = 0.3$. The anisotropy parameter (percentage) ε is defined as follows: (Ben-Menahem & Sena 1990)

$$\varepsilon = \frac{c_{11} - c_{33}}{2c_{33}} \times 100. \tag{28}$$

For Material 2, $\varepsilon = 60.6$ per cent. Now we can examine the anisotropy effect by equalizing the engineering constants in the vertical and horizontal directions to: (1) a mean value to construct a similar artificial isotropic material; that is, $E = E' = 200$ GPa, $\nu = \nu' = 0.2$ and (2)
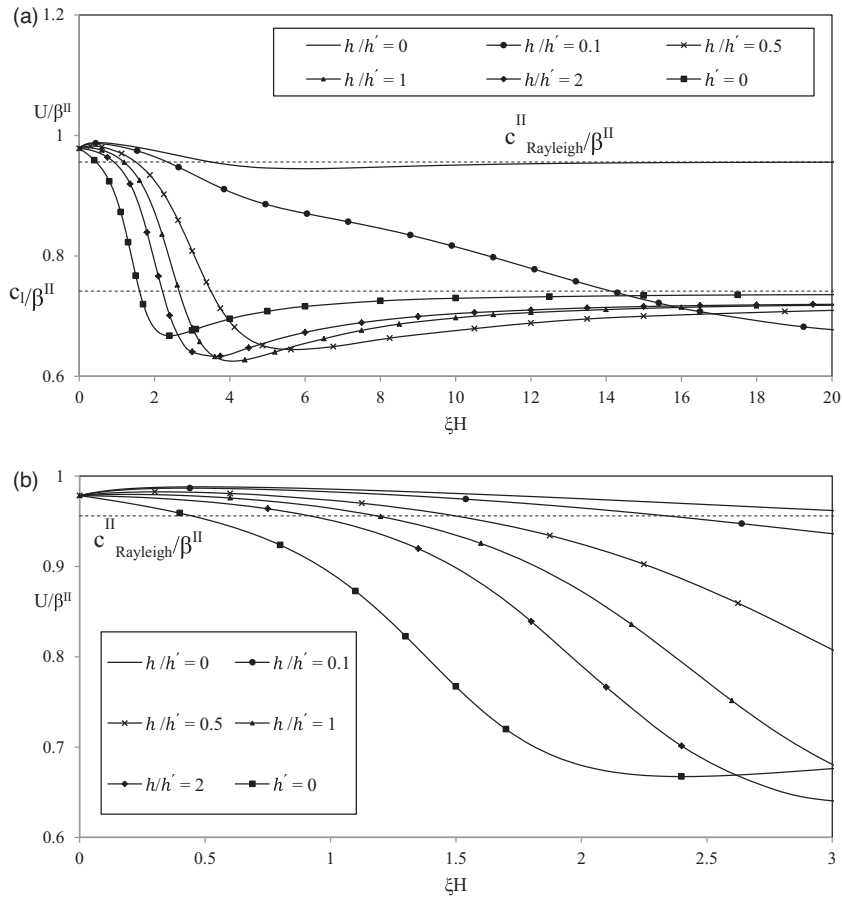
Figure 11. (a) Rayleigh and Stoneley (Scholte) wave group velocity dispersion curves for six values of layer thickness ratios in Model 4. (b) Zoomed-in version of Rayleigh and Stoneley (Scholte) wave group velocity dispersion for low dimensionless wavenumbers in Model 4.
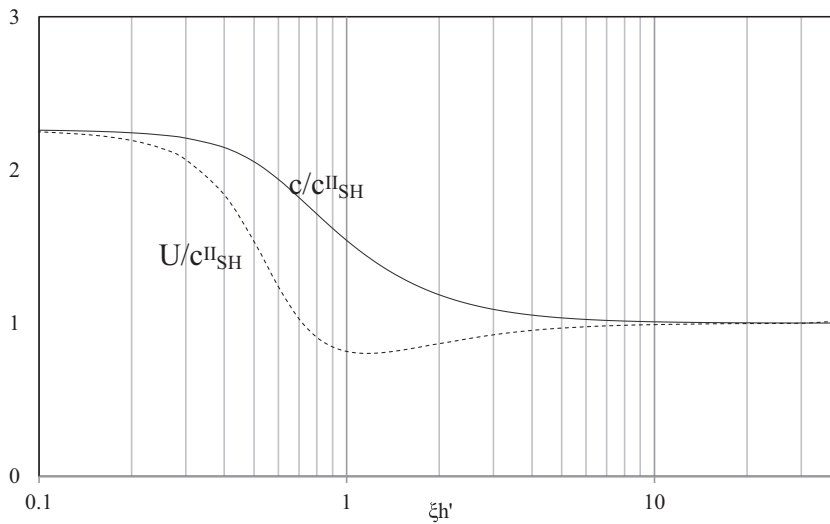

Figure 12. Phase and group velocity dispersion curves for Love wave in Model 1.

to values $E = E' = 100$ GPa and $v = v' = 0.1$. These values give the respective isotropic elastic constants for the first isotropic case (1) as $c_{11} = c_{33} = 222$ GPa, $c_{12} = c_{13} = 55.6$ GPa, $c_{33} = c_{44} = 83.3$ GPa and for the second one (2) as $c_{11} = c_{33} = 134.6$ GPa, $c_{12} = c_{13} = 57.7$ GPa, $c_{33} = c_{44} = 38.5$ GPa. For three values of layer thicknesses, the respective normalized velocity dispersion curves of Rayleigh waves are presented in Figs 14–16, respectively for thickness ratios of $h/h' = 1$, 2 and $h' = 0$. Fig. 17 provides the comparison of Love wave dispersion in the two described models. From the figures, it can be generally appreciated that transverse isotropy plays a considerable role in the phase and group velocity dispersion of surface waves. This can be observed whether a solid middle layer exists or not and for both Rayleigh-Scholte and Love wave dispersion. In the current case, the anisotropy has resulted in a lesser value of group velocity occurring in a greater value
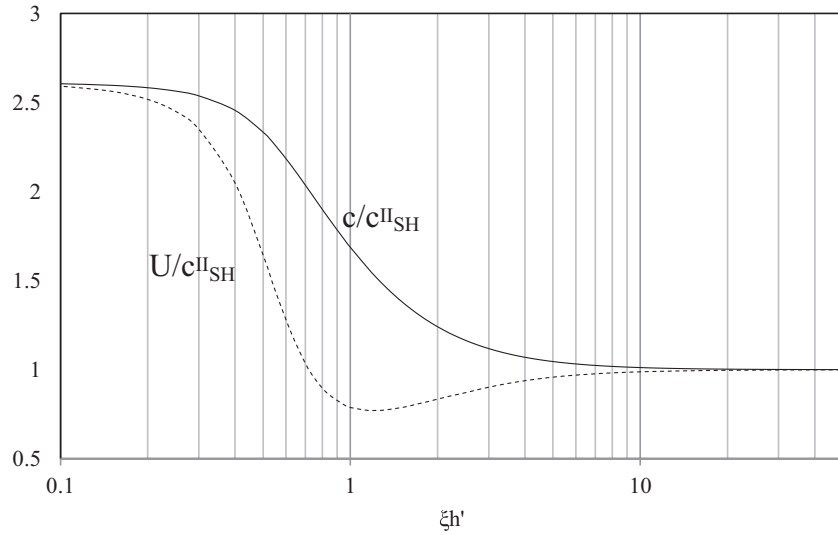
Figure 13. Phase and group velocity dispersion curves for Love wave in Model 3.
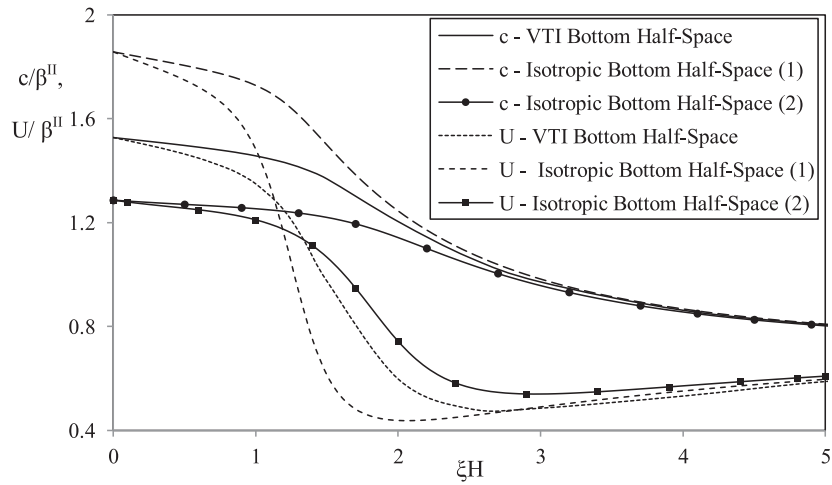

Figure 14. Comparison of Rayleigh wave velocity dispersion curves for isotropic and anisotropic materials as the bottom half-space for $h = h'$.
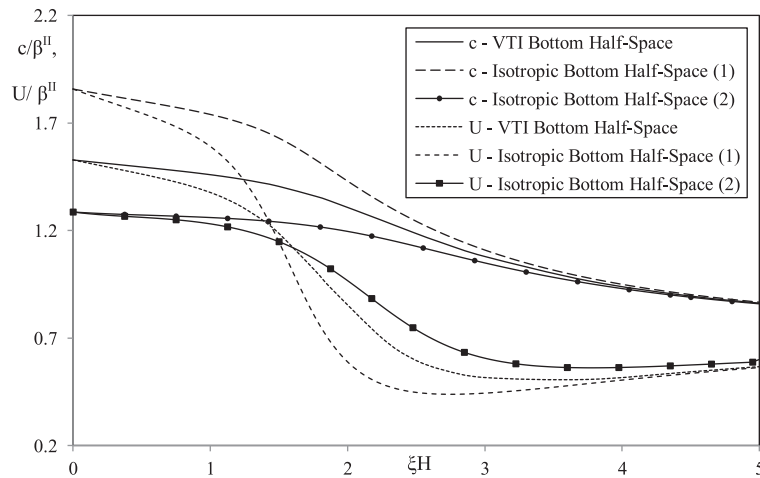

Figure 15. Comparison of Rayleigh wave velocity dispersion curves for isotropic and anisotropic materials as the bottom half-space for $h = h'/2$.
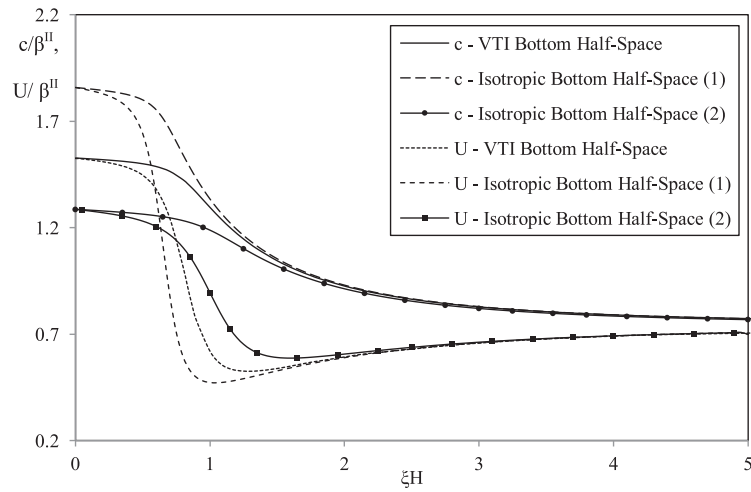
Figure 16. Comparison of Rayleigh wave velocity dispersion curves for isotropic and anisotropic materials as the bottom half-space for $h' = 0$.
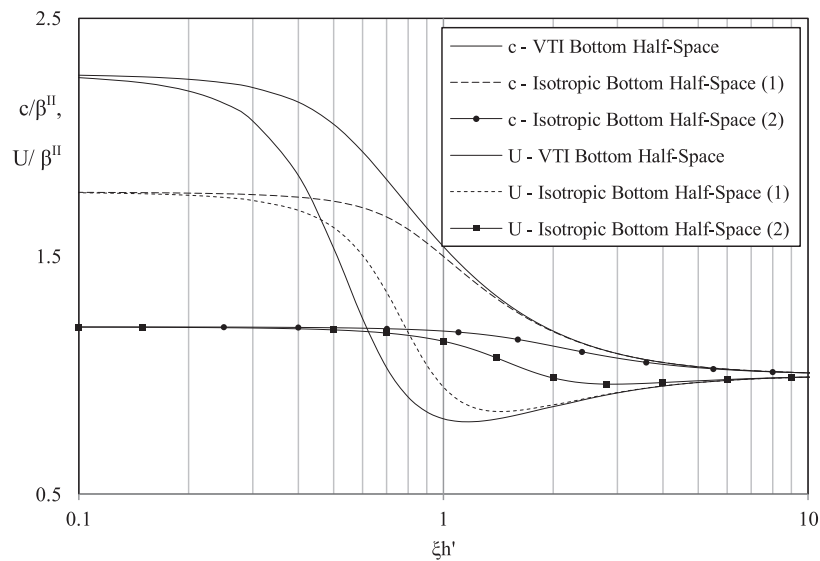

Figure 17. Comparison of Love wave velocity dispersion curves for isotropic and anisotropic materials as the bottom half-space (normalized relative to c_{SH}^{II}).

of dimensionless wavenumber. The effect of anisotropy is most apparent where the layer thickness H is somewhat small compared to the wavelength; that is in smaller dimensionless wavenumbers and frequencies. Moreover, the figures show that as the normalized phase velocity of the Rayleigh wave approaches unity (surface wave velocity gets close to the value of the SV wave in the middle layer), the curves converge to each other rapidly and the effect of this change in the bed material decreases. For the normalized phase velocity values less than unity, the difference between the two cases almost disappears. This suggests that in this part of the curves, it is the upper layers that mainly control the surface wave velocity. For the group velocity curves, this does not occur at the normalized group velocity close to unity, but occurs approximately in the same dimensionless wavenumber as for which normalized phase velocity is close to unity.

6 CONCLUSION

In this paper, we have studied the phase- and group velocity dispersion of elastic waves in a model comprising a homogeneous finite liquid layer lying over a transversely isotropic solid layer which is underlain by a dissimilar transversely isotropic half-space. The Hankel transform in the radial direction and a Fourier series expansion in the azimuthal direction, combined with the aid of potential functions, were used to solve the partial differential equations for the particle displacement. The dispersive characteristics of different types of interface waves are obtained by deriving two frequency equations, one for the Love wave phase velocity and the other for the remaining waves (Rayleigh, Scholte and, Stoneley). Numerical examples are investigated to illustrate the group and phase velocity behaviour for different combinations of material properties and layer thicknesses. The results for various special cases are compared with previously published solutions to confirm the validity of our approach.

The general shape of the dispersion curves depend on the materials properties constituting the models: layer thicknesses, Rayleigh wave velocity of the half-space, P, SH, SV wave velocities of the solids and the *P*-wave velocity of the liquid layer. The shape can be quite different for various combinations of materials as is apparent from the results presented for several numerical examples. The important effect of even a thin liquid layer with respect to the wavelength, as well as the underlying material properties on the dispersion characteristics can be observed from the diagrams presented for various materials. The ratio of the thicknesses of the liquid to that of the VTI solid is clearly important, especially for not too large ξh values. The results are also very sensitive to the existence of a transversely isotropic solid layer lying between the liquid and the substratum. Phase velocity dispersion curves may have more than one extremal point, depending on the thickness of the liquid layer and material properties. The group velocity dispersion curves may indicate several local maxima and minima, which also depend on the aforementioned parameters. For the studied models, the absolute minimum value of the group velocity occurs at lower dimensionless wavenumbers, when the liquid layer is present.

The sensitivity of results to the anisotropy of the solid layer material is examined for three thickness ratios of the liquid and middle VTI layer. The curves show the importance of the anisotropy, especially when the velocity of the surface wave is greater that the value of the SH wave in the middle layer.

The dispersion curves can be used in an inverse sense to reconstruct the material properties although that is not pursued here. Furthermore, the formulation can be extended to calculate the elastodynamic response of the system subjected to dynamic excitations. Research on this topic is currently underway.

ACKNOWLEDGEMENTS

REFERENCES

Abubakar, I. & Hudson, J.A., 1961. Dispersive properties of liquid overlying an aelotropic half-space, *Geophys. J. R. astr. Soc.,* **5,** 217–229.

Barnett, D.M., 2000. Bulk, surface, and interfacial waves in anisotropic linear elastic solids, *Int. J. Solids. Struct.,* **37,** 45–54.

Ben-Menahem, A. & Sena, A.G., 1990. Seismic source theory in stratified anisotropic media, *J. geophys. Res.,* **95,** 15 395–15 427.

Biot, M.A., 1952. The Interaction of Rayleigh and Stoneley Waves in the Ocean Bottom, *Bull. seism. Soc. Am.,* **42,** 81–92.

Boxberger, T., Picozzi, M. & Parolai, S., 2011. Shallow geology characterization using Rayleigh and Love wave dispersion curves derived from seismic noise array measurements, *J. appl. Geophys.,* **75,** 345–354.

Buchwald, V.T., 1961. Rayleigh waves in transversely isotropic media, *Q. J. Mech. Appl. Math.,* **14,** 293–317.

Cagniard, L., 1962. *Reflection and Refraction of Progressive Waves,* translated and revised by Fiinn, E.A. & Dix, C.M., McGraw-Hill.

Crampin, S., 1981. Review of wave motion in anisotropic and cracked elastic media, *Wave Motion,* **3,** 343–391.

Eskandari-Ghadi, M., 2005. A complete solutions of the wave equations for transversely isotropic media, *J. Elast.,* **81,** 1–19.

Ewing, W.M., Jardetzky, W.S. & Press, F., 1957. *Elastic Waves in Layered Media,* McGraw-Hill Book Co. Inc.

Favretto-anres, N. & Rabau, G., 1997. Excitation of the Stoneley-Scholte wave at the boundary between an ideal fluid and a viscoelastic solid, *J. Sound Vibr.,* **20,** 193–208.

Flores-Mendez, E., Carbajal-Romero, M., Flores-Guzman, N., Sanchez-Martinez, R. & Rodríguez-Castellanos, A., 2012. Rayleigh's, Stoneley's, and Scholte's interface waves in elastic models using a boundary element method, *J. appl. Math.,* **2012,** doi:10.1155/2012/313207.

Haskell, N.A., 1953. The dispersion of surface waves in multilayered media, *Bull. seism. Soc. Am.,* **43,** 17–34.

Kerner, C., Dyer, B. & Worthington, M., 1989. Wave propagation in a vertical transversely isotropic medium: field experiment and model study, *Geophys. J. Int.,* **97,** 295–309.

Khojasteh, A., Rahimian, M., Eskandari, M. & Pak, R.Y.S., 2008a. Asymmetric wave propagation in a transversely isotropic half-space in displacement potentials, *Int. J. Eng. Sci.,* **46,** 690–710.

Khojasteh, A., Rahimian, M. & Pak, R.Y.S., 2008b. Three-dimensional dynamic Green's functions in transversely isotropic bi-materials, *Int. J. Solids. Str.,* **45,** 4952–4972.

Khojasteh, A., Rahimian, M., Pak, R.Y.S. & Eskandari, M., 2008c. Asymmetric dynamic Green's functions in a two-layered transversely isotropic half-space, *J. Eng. Mech. ASCE,* **134,** 777–787.

Khojasteh, A., Rahimian, M., Eskandari, M. & Pak, R.Y.S., 2011. Three-dimensional dynamic Green's functions for a multilayered transversely isotropic half-space, *Int. J. Solids. Str.,* **48,** 1349–1361.

Khojasteh, A., Rahimian, M. & Eskandari, M., 2013. Three-dimensional dynamic Green's functions in transversely isotropic tri-materials, *J. appl. Math. Model.,* **37,** 3164–3180.

Kiełczyński, P., Szalewski, M. & Balcerzak, A., 2014. Inverse procedure for simultaneous evaluation of viscosity and density of Newtonian liquids from dispersion curves of Love waves, *J. appl. Phys.,* **116,** 044902, doi:10.1063/1.4891018.

Kuznetsov, S., 2006. Love waves in layered anisotropic media, *J. appl. Math. Mech.,* **70,** 127–166.

Nadri, D., Sarout, J., Bona, A. & Dewhurst, D., 2012. Estimation of the anisotropy parameters of transversely isotropic shales with a tilted symmetry axis, *Geophys. J. Int.,* **190,** 1197–1203.

Ostoja-Starzewski, M., 1987. Propagation of Rayleigh, Scholte and Stoneley waves along random boundaries, *Probabilist. Eng. Mech.,* **2,** 64–73.

Padilla, F., de Billy, M. & Quentin, G., 1999. Theoretical and experimental studies of surface waves on solid–fluid interfaces when the value of the fluid sound velocity is located between the shear and the longitudinal ones in the solid, *J. acoust. Soc. Am.,* **106,** 666–673.

Payton, R.G., 1983. *Elastic Wave Propagation in Transversely Isotropic Media,* Martinus.

Poulos, H.G. & Davis, E.H., 1974. *Elastic Solutions for Soil and Rock Mechanics,* Wiley.

Rahimian, M., Eskandari-Ghadi, M., Pak, R.Y.S. & Khojasteh, A., 2007. Elastodynamic potential method for transversely isotropic solid, *J. Eng. Mech., ASCE,* **133,** 1134–1145.

Sharma, M.D., 1999. Dispersion in oceanic crust during earthquake preparation, *Int. J. Solids Struct.,* **36,** 3469–3482.

Sharma, M.D., Kumar, R. & Gogna, M.L., 1990. Surface wave propagation in a transversely isotropic elastic layer overlying a liquid saturated porous solid half-space and lying under the uniform layer of liquid, *Pure. appl. Geophys.,* **133,** 523–539.

Sharma, M.D., Kumar, R. & Gogna, M.L., 1991. Surface wave propagation in a liquid saturated porous solid layer overlying a homogeneous transversely isotropic half-space and lying under a uniform layer of liquid, *Int. J. Solids. Struct.,* **127,** 1255–1267.

Stoneley, R., 1924. Elastic waves at the surface of separation of two solids, *Proc. R. Soc., Lond., A,* **106,** 416–428.

Stoneley, R., 1926. The effect of ocean on Rayleigh waves, *Mon. Not. R. astro. Soc. Geophys. Suppl.,* **1,** 349–356.

Stoneley, R., 1949. The seismological implications of aeolotropy in continental structures, *R. astr. Soc. Mon. Notices., Geophys. Supp.,* **5,** 343–353.

Synge, J.L., 1957. Elastic waves in anisotropic media, *J. Math. Phys.,* **35,** 323–334.

Tolstoy, L., 1954. Dispersive properties of a fluid layer overlying a semi-infinite elastic solid, *Bull. seism. Soc. Am.,* **44,** 493–512.

Zhou, B. & Greenhalgh, S., 2008. Velocity sensitivity of seismic body waves to the anisotropic parameters of a TTI-medium, *J. geophys. Eng.,* **5,** 245–255.

Zhou, B., Greenhalgh, M. & Greenhalgh, S.A., 2009. 2.5-D/3-D resistivity modelling in anisotropic media using Gaussian quadrature grids, *Geophys. J. Int.,* **176,** 63–80.

Zhou, B., Greenhalgh, S. & Greenhalgh, M., 2012. Wavenumber sampling strategies for 2.5-D frequency-domain seismic wave modelling in general anisotropic media, *Geophys. J. Int.,* **188,** 223–238.